



OPEN **iPSC-derived human sensory neurons reveal a subset of TRPV1 antagonists as anti-pruritic compounds**

Shermaine Huiping Tay¹, Jeremy Kah Sheng Pang¹, Winanto Ng¹, Chong Yi Ng¹, Zi Jian Khong¹, Zheng-Shan Chong¹, Boon Seng Soh¹ & Shi-Yan Ng^{1,2,3}✉

Signaling interplay between the histamine 1 receptor (H1R) and transient receptor potential cation channel subfamily V member 1 (TRPV1) in mediating histaminergic itch has been well-established in mammalian models, but whether this is conserved in humans remains to be confirmed due to the difficulties in obtaining human sensory neurons (SNs) for experimentation. Additionally, previously reported species-specific differences in TRPV1 function indicate that use of human SNs is vital for drug candidate screening to have a higher chance of identifying clinically effective TRPV1 antagonists. In this study, we built a histamine-dependent itch model using peripheral SNs derived from human induced pluripotent stem cells (hiPSC-SNs), which provides an accessible source of human SNs for pre-clinical drug screening. We validated channel functionality using immunostaining, calcium imaging, and multielectrode array (MEA) recordings, and confirmed the interdependence of H1R and TRPV1 signalling in human SNs. We further tested the amenability of our model for pre-clinical studies by screening multiple TRPV1 antagonists in parallel, identifying SB366791 as a potent inhibitor of H1R activation and potential candidate for alleviating histaminergic itch. Notably, some of the results using our model corroborated with efficacy and side effect findings from human clinical trials, underscoring the importance of this species-specific platform. Taken together, our results present a robust in vitro human model for histaminergic itch, which can be used to further interrogate the molecular basis of human SN function as well as screen for TRPV1 activity-modifying compounds for a number of clinical indications.

Keywords Sensory neurons, Human pluripotent stem cells, MEA, Itch, Histamine receptor, TRPV1, TRPV1 antagonist

Pruritus (itch) and pain are distinct sensations that share overlapping mediators and receptors^{1,2}. Sensory neurons, especially those expressing transient receptor potential (TRP) channels such as TRPV1, contribute to pain mediation. However, TRPV1, a multi-functional channel, is also implicated in thermoregulation and the mediation of histamine-induced itch. In the process of itch propagation, histamine binds to histamine 1 receptor (H1R) and activates heterotrimeric G-protein, initiating a downstream signaling cascade. This cascade involves the opening of transient receptor potential cation channel subfamily V member 1 (TRPV1) and voltage gated sodium channels, initiating the propagation of signals³. Even though TRPV1's downstream role of H1R in relaying histamine-induced itch has been extensively studied in surrogate mammalian models such as in mice and rats³⁻⁸, our understanding of this signaling pathway in humans is still developing. While ethical and technical challenges persist in isolating primary human dorsal root ganglia (DRG) neurons, recent studies have successfully utilized human DRGs to investigate their functionality and gene expression⁹⁻¹². Nonetheless, the development of differentiation protocols that generate functional peripheral sensory neurons from human pluripotent stem cells (hiPSC-SNs)¹³⁻¹⁶ offers a scalable, ethically viable, and physiologically relevant model for studying sensory pathways, including pruritus, in humans.

¹Institute of Molecular and Cell Biology (IMCB), Agency for Science, Technology and Research (A*STAR), 61 Biopolis Drive, Proteos, Singapore 138673, Republic of Singapore. ²Yong Loo Lin School of Medicine (Physiology), National University of Singapore, Singapore 117456, Republic of Singapore. ³National Neuroscience Institute, Singapore 308433, Republic of Singapore. ✉email: syng@imcb.a-star.edu.sg

TRPV1 is an attractive therapeutic target of pruritus as it is also involved as a downstream mediator of another key atopic dermatitis (AD) inflammatory marker, i.e. IL-31¹⁷. Some TRPV1 targeting anti-pruritic agents that have been tested in clinical trials include TRPV1 agonists and capsaicin, which acts through chronic channel desensitization¹⁸. TRPV1 antagonists acting through direct or indirect channel inactivation, such as Pegcantratinib and Asivatrep have also been carefully described^{19,20}. Despite the interest, very few TRPV1 antagonists have actually advanced from animal testing to clinical trials as they tend to elicit adverse effects of hyperthermia²¹. This major caveat is further compounded by species-specific differences in TRPV1-mediated thermoregulation, which led to varied hyperthermic responses between different mammalian species and in human clinical trials^{21,22}. Because of these hyperthermic side effects, the therapeutic applications of TRPV1 antagonists as anti-pruritic agents are limited.

To overcome these limitations, we built a humanized histamine-dependent itch model using sensory neurons derived from human pluripotent stem cells (hiPSC-SNs) that allows robust validation of neuronal activity downstream of H1R and TRPV1. Single-cell RNA-sequencing revealed enrichment of sensory neuron markers in the neuronal cluster within our culture. We demonstrated that hiPSC-SNs express functional TRPV1 channels activated by heat (42 °C) and capsaicin, along with functional H1R activated by histamine. Immunostaining and calcium imaging unveiled a subset of sensory neurons co-expressing TRPV1 and H1R. Electrophysiological analysis further affirmed a conserved H1R and TRPV1 signaling pathway in our hiPSC-SNs. In a proof-of-concept study, we evaluated five known hyperthermic and thermal-neutral TRPV1 antagonists, revealing varying potencies against histamine-mediated activation in our hiPSC-SNs for the first time. These findings suggest the potential development of hiPSC-SNs into a drug discovery platform for identifying anti-itch compounds.

Materials and methods

Differentiation of hiPSC toward sensory neurons

We used the hiPSC line (BJ-iPS) that was reprogrammed from BJ fibroblasts (ATCC) using modified mRNAs²³. These were directed towards a sensory neuron fate according to our protocol described previously²⁴. Briefly, hiPSCs were plated onto Matrigel-coated plates at a density of 50,000 cells/cm² on day 1 and induced into an anterior neuroectodermal lineage with 0.5 µM LDN-193,189 (Stemcell Technologies) and 10 µM SB431542 (Miltenyi Biotec) for synergistic dual SMAD inhibition. At day 3, 3 µM Wnt agonist CHIR99021 (Miltenyi Biotec) coupled with 5 µM FGF inhibitor, SU5402 (Stemcell Technologies) were added to pattern neural progenitors towards a neural crest fate. 5 µM DAPT (Stemcell Technologies) was additionally used to block Notch signalling and encourage differentiation of progenitors into neurons. From day 6 to 11, LDN-193,189 and SB431542 were withdrawn. Depending on the downstream experiments, differentiating SNs were passaged between day 6 and 8 using Accutase (Stemcell Technologies) and seeded onto Matrigel-coated plates of different formats and at various densities (24-well MEA plate: 125,000 cells/cm²; 8-chamber, 12-, 24-well plate: 80,000 cells/cm²). Finally to promote maturation of sensory neurons, neurotrophic factors including 20 ng/mL BDNF (Miltenyi Biotec), 20 ng/mL GDNF (Miltenyi Biotec), 20 ng/mL NGF-β (Miltenyi Biotec) and 10 ng/mL ascorbic acid (Sigma Aldrich) were added from day 11 onwards. 0.5 µM AraC treatment was performed between day 11 and 13 to eliminate progenitor cells in the culture. Sensory neuron basal media was prepared using 250 mL of DMEM/F12 (Bio-Rad), 250 mL of Neurobasal media (Miltenyi Biotec), supplemented with MACS Neurobrew-21 w/o Vitamin A, 0.5% GlutaMAX and 1% N2 supplement.

Differentiation of hiPSC toward motor neurons

Human induced pluripotent stem cells (hiPSCs; BJ-iPSC cell line) were directed towards a motor neuron fate according to our protocol described previously²⁴.

Single-cell dissociation

For cell detachment, 46-day old hiPSC-SNs were treated with Accutase for 8 min at 37 °C and transferred into 15 mL conical tube before topping up with dPBS to 10 mL and centrifuging at 1000 rpm for 3 min. The supernatant was discarded and hiPSC-SNs within the pellet were dissociated using papain (Worthington Biochemical) according to manufacturer's instructions. Briefly, papain digestion was carried out at 37 °C with constant agitation for 30 min and with manual pipetting done every 10 min. Cells were spun down at 1000 rpm for 3 min and the supernatant was discarded. The reaction was stopped by re-suspension and incubation in diluted DNase/albumin-inhibitor solution at 37 °C for 5 min before centrifugation at 1000 rpm for 3 min and discarding the supernatant. Finally, dissociated cells were resuspended into 500 µL Sensory neuron maturation medium to a concentration of ~ 320 cells/µL and filtered through a 40 µm cell strainer to remove any remaining undissociated cell clumps.

Single cell RNA-seq library preparation and sequencing

The single-cell suspensions were assessed by acridine orange/propidium iodide staining to contain a cell viability of 97.2%. Using the GEXSCOPE kit, the cells were loaded into microwells of a microfluidic SCOPE-chip and lysed to release mRNA hybridizing to unique barcode sequences on the bead in the same well. The hybridized mRNA was reverse transcribed into cDNA and amplified. The resulting amplified cDNA was fragmented, ligated to adaptors and processed to construct a sequencing library compatible with the Illumina sequencing platform. The raw single cell transcriptomics data is publicly available at Gene Expression Omnibus (GEO) with an accession number GSE256435.

Single-cell RNA-seq data analysis

Raw sequencing reads were processed by Telescope pipeline with default parameters to generate filtered single-cell gene expression matrix files (<https://github.com/singleron-RD/CeleScope>). R package Seurat (v4.1.1)

was used to further process the gene expression matrix files²⁵. Quality control was first performed, and cells containing between 100 and 7500 unique feature counts with less than 20% mitochondrial transcripts were kept. Genes expressed in less than 5 cells were also removed. After quality control, 13,410 cells remained, and their expression data was normalized and scaled. FindVariableFeatures was used to identify the highly variable genes which was used to conduct principal component analysis. The ElbowPlot function was used to suggest the dimensionality of the dataset, and a value of 20 was used. FindNeighbors and FindClusters were used to cluster the cells using the shared nearest neighbor graphs. A range of resolutions were tested, and the value of 0.3 was used, which resulted in 8 clusters. Uniform Manifold Approximation and Projection dimensionality reduction was performed using RunUMAP for visualization. To infer the identities of the clusters, FindAllMarkers was used to identify the most upregulated genes in each cluster. DotPlot was used to aid in the visualization in the most upregulated genes from each cluster. In addition, commonly accepted gene markers (such as PRPH, ISL1, STMN2) was used to further support the identities of the neuronal clusters. Clusters 0, 3 and 7 were determined to be neuronal, and contained a total of 5031 cells.

RNA extraction and qPCR

Cells were harvested in Trizol reagent for RNA extraction using RNeasy Mini Kit (Qiagen) according to manufacturer's instructions. cDNA conversion was performed using the high-capacity cDNA Reverse Transcription Kit (Applied Biosystem, USA). Quantitative PCR (qPCR) was performed on QuantStudio 5 Real-Time PCR system using Fast SYBR Master Mix (Applied Biosystems). Gene expression was normalized to *ACTINB* and *GAPDH*. Primers used are listed in Supplementary Table S1.

Immunostaining and image acquisition

Human iPSC-derived sensory neurons were fixed with 4% paraformaldehyde for 15 min, permeabilized with 0.1% Triton X-100 for 20 min and incubated in blocking buffer consisting of 5% FBS and 1% BSA for 2 h at room temperature. Blocking solution were replaced with primary antibody diluted in blocking solution and incubated at 4 °C overnight. The primary antibodies used in this study were rabbit anti-TrkA (1:400; CST, 2510 S), mouse anti-Brn-3a (1:100; Merck Millipore, MAB1585), rabbit anti-Peripherin (1:500; Merck Millipore, AB1530), rabbit anti-Islet 1 (1:500; Abcam, ab109517), rabbit anti-H1 Histamine Receptor (1:500; Alomone, AHR-001), rabbit anti-TRPV1 (1:500; Alomone, ACC-030) and followed by Alexa Fluor-conjugated secondary antibodies (1:1250; Invitrogen). DAPI (0.5 µg/mL) was used for nuclear staining. To capture H1R and TRPV1 co-expression, sequential staining was carried out with thorough washes in between to avoid cross-reactivity of secondary antibodies to the primary antibodies. Fluorescence images were captured with either ZOE Fluorescent Cell Imager (Biorad) or FV1000 confocal microscope (Olympus) using 20x objective.

Preparation of small molecule agonists and antagonists

For agonist preparation, histamine (Sigma, H7125) and capsaicin (Sigma, M2028) were reconstituted in ddH₂O and DMSO to stock concentrations of 100 mM first and then further diluted in media to working concentrations of 25 µM and 0.5 µM, respectively, unless otherwise stated. For antagonist preparation, mepyramine/pyrilamine maleate salt (Sigma, P5514), QX 314 bromide (Hello bio, HB1029), AMG9810 (Sigma, A2731), AMG517 (Cayman, Cay26191), ABT102 (Axon Medchem, Axon 1504), SB366791 (Sigma, S0441), SB705498 (Alomone, S-160) and PAC14028 (MedChemExpress, HY-12777) were reconstituted in DMSO to stock concentrations of 50 mM and then diluted in media to their stated concentrations.

Calcium imaging

Human iPSC-derived sensory neurons that are at least 28 days old were pre-loaded with Calcium 6 Assay Dye (Molecular Devices, R8190) and incubated for 2 h at 37 °C in a 5% CO₂ incubator. All calcium imaging was performed directly in the dye without washing. Fluorescent images were obtained on a Nikon Ti-E Motorized Inverted microscope (SBIC-Nikon Imaging Centre at Biopolis) with a 20x objective and at 488 nm excitation. Exposure timing was set as 30 ms and interval as 500 ms. Baseline activities were measured for 20 s before addition of agonists and recorded for another 3 min. For antagonist testing, neurons were pre-incubated with the inhibitors for 10 min prior to recording. Quantitation was carried out on NIS-Elements software using the General Analysis module. Briefly, the original video file was used to generate an intermediate file containing three channels, i.e. baseline (B), maximum intensity projected (P) and maximum minus baseline (P-B) intensity. Next, the General Analysis function to increase the image contrast, threshold and count was applied to (P) and (P-B) channels in the intermediate file. This generated binary layers which were then converted to regions of interest (ROIs) corresponding to total cell count in (B) channel and agonist-responsive only cells in (P-B) channel. Finally, the ROIs were applied back to the original video file to prune off ROIs that did not accurately map to sensory neurons excitabilities. For experiment involving non-differentiated cells, BJ-iPSC cells were pre-loaded with Calcium 6 Assay Dye and incubated for 2 h at 37 °C in a 5% CO₂ incubator. Fluorescent images were captured using both the EVOS M5000 Imaging System and the Varioskan LUX Multimode Microplate Reader, employing an excitation wavelength of 488 nm. Exposure durations were configured at 30 ms for the EVOS M5000 and 100 ms for the Varioskan LUX, with a common interval of 1 s.

Multielectrode array (MEA) electrophysiology

All MEA extracellular potential recordings were carried out on the 24-well glass bottom Multiwell-MEA system (Multi Channel Systems), which contains 12 electrodes per well. MEA plates were pre-coated with Matrigel to promote neural cell attachment, and differentiating neurons between day 6 and 8 were seeded at 125,000 cells/cm² and allowed to continue to mature until at least 28 days old, when recordings were taken. For standard assay without noxious heat (recorded at a consistent temperature of 37 °C), baseline condition was recorded for

5 min prior to recording for another 5 min in the presence of agonist. Neurons were rested for 45 min before being incubated with antagonists for 10 min and then recorded for another 5 min in the additional presence of an agonist. This is with the exception for QX 314 bromide experiments where the neurons were incubated with both antagonist and agonist to silence selective subsets of neurons before excitation with a second agonist. The MEA plates were always stabilized on the reader for 3–5 min prior to recording. For assay involving single time heating, extracellular potentials were recorded for 20 min as the neurons were heated from 37 to 42 °C and gradually cooled back to 37 °C. For repeated heating assays, 45 min rest intervals were added in between heating and burst spike count was only tabulated between the 8 and 9th minute where temperature is stabilized at 42 °C. All raw data recorded was analyzed on the Multiwell-Analyzer software. Burst spike count was quantified as the total number of spikes that occurred during burst events. Bursts were identified as at least four densely packed spikes with a maximum inter-spike interval of 50 ms, minimum inter-burst interval of 100 ms and a minimum burst duration of 50 ms. Spikes are set as signals with rising and falling edges beyond the threshold of 5 standard deviation.

Statistical analyses

All data shown represent at least three biological replicates except for experiments described in Fig. 3C, F, I. Shapiro–Wilk tests were performed on all datasets to determine for normality. When the normality assumption is not met, non-parametric tests were performed instead. For comparisons between three or more conditions, statistical significance was determined by Friedman test with Dunn's multiple comparisons test using Graphpad Prism, unless otherwise specified. For comparisons between two conditions, statistical significance was determined by unpaired parametric Student T-test or by non-parametric Mann-Whitney test.

Results

Single cell transcriptomics reveal robust generation of sensory neurons and other neural crest cell types from human iPSCs

Peripheral sensory neurons were derived from iPSCs by first patterning them towards a neural crest fate, followed by further specification towards peripheral neurons. Following a 45-day protocol previously established in the lab (Fig. 1A)²⁴, the neuronal culture was characterized by single cell RNA-sequencing (scRNA-seq), which revealed a diversity of neural crest-derived cell types (Fig. 1B). Within this heterogeneous population, we identified neural crest progenitor cells based on their expression of Nestin (NES) and Slug (SNAI2), Schwann cells expressing S100B and myelin protein zero (MPZ), satellite glia cells expressing FABP7 and SLC1A3, as well as several neuronal clusters marked by stathmin 2 (*STMN2*) and neurofilament light chain (*NEFL*) (Fig. 1C) (Supplementary Fig. 1A). These neuronal clusters are also enriched for sensory neuron markers such as peripherin (*PRPH*) and Islet-1 (*ISL1*), confirming that peripheral sensory neurons can be robustly derived from human iPSCs (Fig. 1C).

To validate the scRNA-seq data, quantitative PCR was used to profile transcript expression across time. We were able to detect consistent mRNA expression of sensory neuron markers such as *TRKA*, *PRPH*, *BRN3A* and *ISL1* as early as day 15 (Fig. 1D and Supplementary Fig. 1B) through day 49 (Supplementary Fig. 1D), which we further confirmed this with immunostaining (Fig. 1E). By day 28, mRNA expression of G-protein coupled (metabotropic) receptor *H1R* and specific channels such as *TRPV1*, *SCN9A* and *SCN11A* were also detected (Fig. 1F and Supplementary Fig. 1C), with *H1R* and *TRPV1* demonstrating increased expression as the differentiation period extended to 43 days (Supplementary Fig. 1E). We continued to mature these hiPSC-SNs in vitro until day 50, and immunostaining analyses revealed robust co-expression of the histamine receptor type 1 (*H1R*) and transient receptor potential vanilloid-1 (*TRPV1*) (Fig. 1G). It has been shown previously that *H1R* exerts itch by activating *TRPV1*^{4,5,8}. Therefore, the co-expression of *H1R* and *TRPV1* in our iPSC-SNs indicate the successful derivation of sensory neurons that can model itch, as well as identify anti-pruritic compounds.

hiPSC-SNs show increased neuronal activity in response to histamine and TRPV1 agonists

To characterize the function of these hiPSC-SNs, we first performed calcium imaging using the Calcium-6 dye, and recorded the changes in calcium fluxes pre- and post-treatment with 25 μM histamine (*H1R* agonist) or 0.5 μM capsaicin (*TRPV1* agonist) (Fig. 2A). Non-differentiated BJ-iPSC cells showed no calcium response (Supplementary Fig. 2A, B), while hiPSC-SNs exhibited a robust response to histamine and capsaicin, which was abolished by co-treatment with the *H1R* antagonist mepyramine (Mepy) or the *TRPV1* antagonist AMG9810 respectively (Fig. 2B, C). Expanding on this study, we next measured neuronal network activities of hiPSC-SNs using the multielectrode array (MEA). Upon treatment with histamine, hiPSC-SNs exhibited a 2.5-fold increase in burst firing, which was reversibly suppressed by mepyramine (Fig. 2D). Similarly, hiPSC-SNs exposed to capsaicin showed a 6-fold increase in burst firing, which was also reversibly inhibited by AMG9810 (Fig. 2E). We used a lower concentration of capsaicin (0.5 μM) compared to previous hiPSC-SNs studies (1–10 μM)^{14,26–28} to avoid acute *TRPV1* desensitization, which occurs at higher doses (Supplementary Fig. 2C). We further demonstrated that this increase in burst firing in response to capsaicin was specific to iPSC-SNs by differentiating the iPSCs towards spinal motor neurons, which do not express *TRPV1*, and found no changes in burst firing in the presence of capsaicin (Supplementary Fig. 2D).

Since *TRPV1* is also a thermosensitive channel, we investigated the changes in neuronal bursts in the hiPSC-SNs in response to temperatures ranging from 37 to 42 °C. As expected, increased neuronal bursts were observed at 42 °C, and this was abolished by either removal of the heat insult or treatment with 10 μM AMG9810 (Fig. 2F). To understand if burst firing patterns of hiPSC-SNs change over time, weekly MEA recordings of the hiPSC-SNs were taken. Intrinsic burst activity as well as capsaicin-responsive neuronal bursts followed a normal distribution over time, where maximal activity was observed between days 37 and 51 (Supplementary Fig. 2E). Therefore, subsequent experiments were performed on hiPSC-SNs between days 37 and 51. Altogether, our data

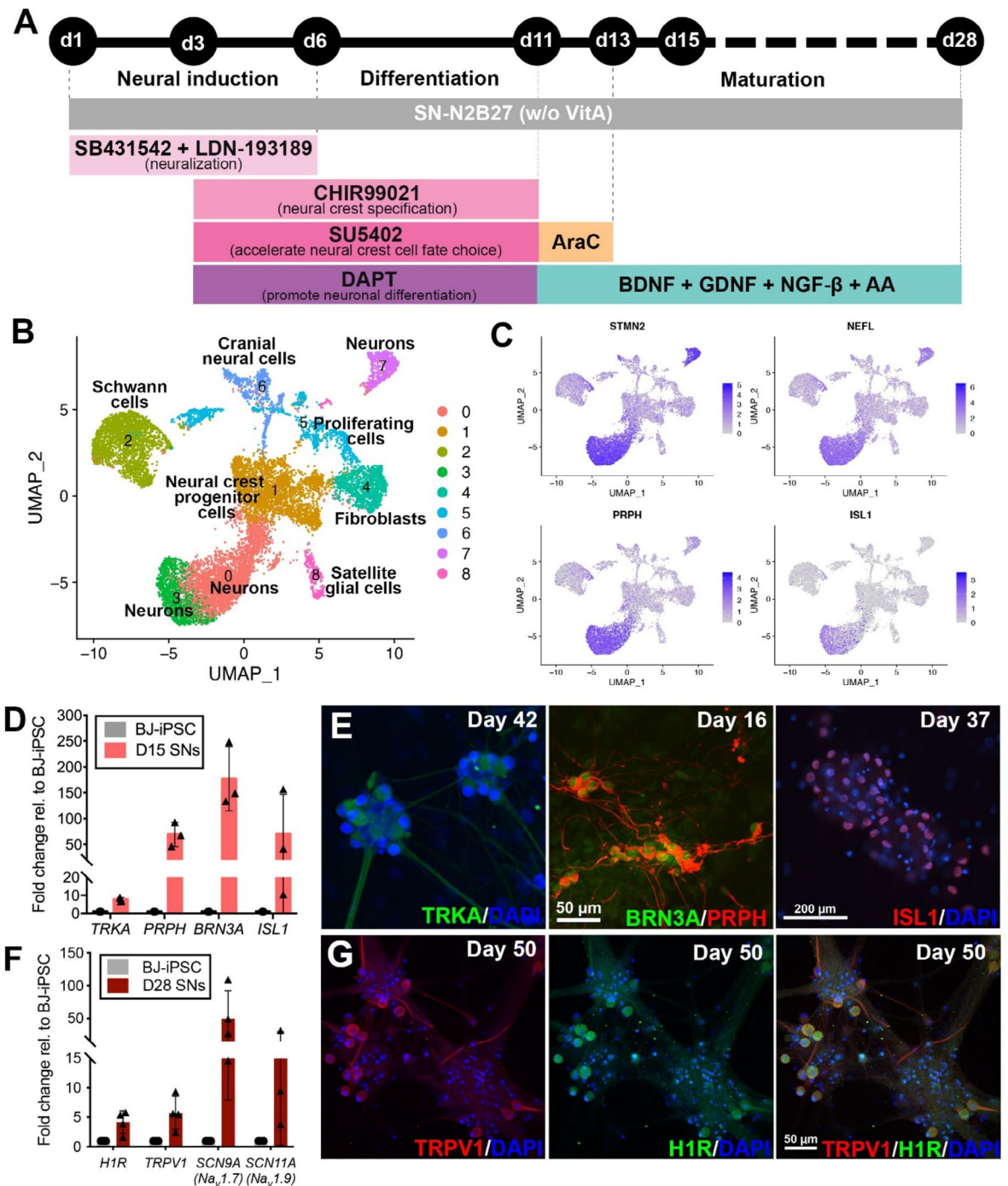
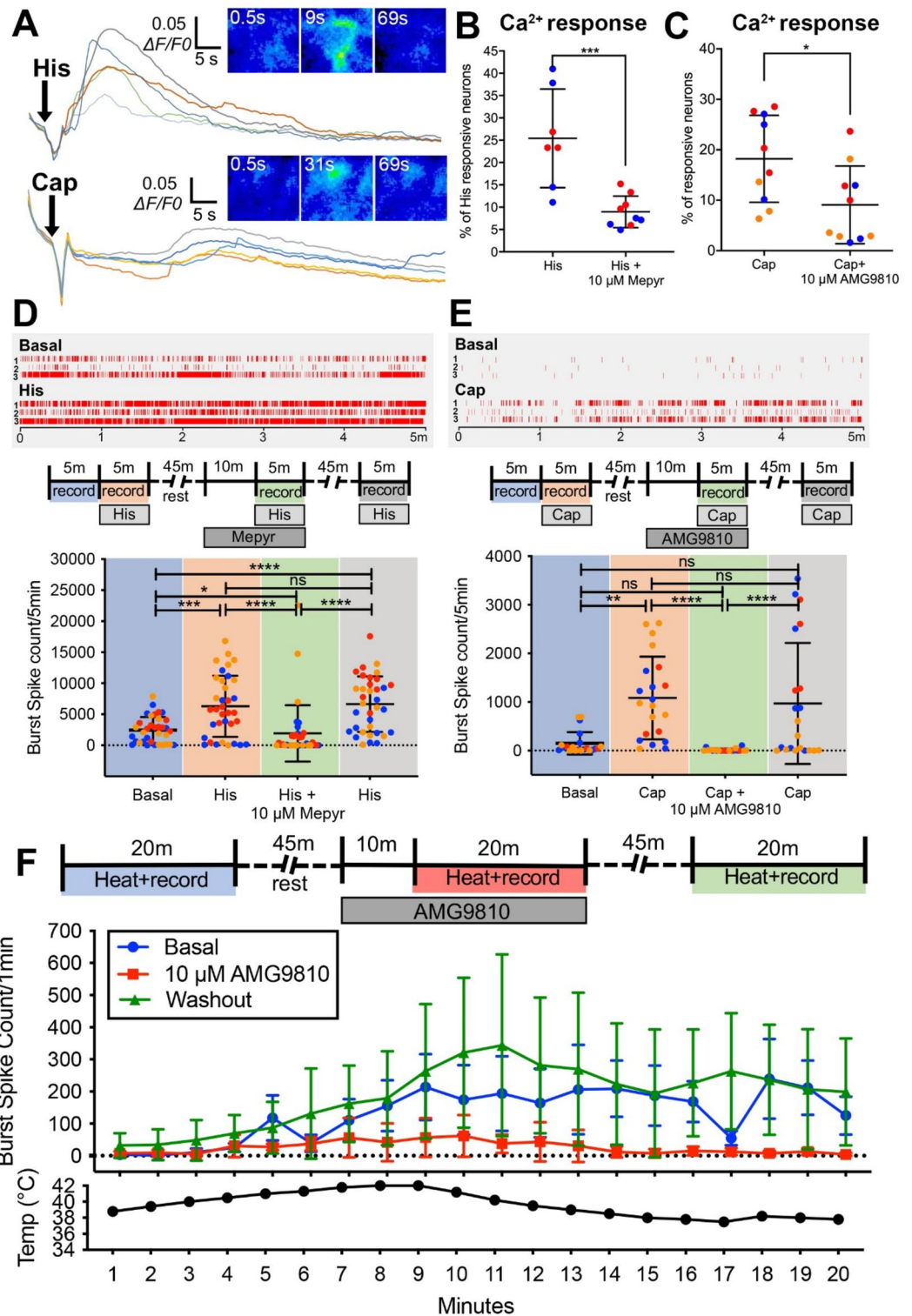


Fig. 1. Derivation of hiPSC-SNs and characterization of H1R and TRPV1 signalling elements. **(A)** Directed differentiation protocol to obtain Sensory neurons from human induced pluripotent stem cells (hiPSC-SNs) as early as within 28 days. **(B,C)** Identification of cell types present in 45-day old hiPSC-SN culture using single cell RNA-seq. UMAP plot showing the 8 clusters identified **(B)**. UMAP plots of the expression of gene markers that were used to label neuronal clusters (*STMN2* and *NEFL*) and Sensory neuron clusters (*PRPH* and *ISL1*) **(C)**. **(D)** qPCR analysis in hiPSC-SNs showing upregulation of SN canonical markers, i.e. *TRKA*, *PRPH*, *BRN3A* and *ISL1* relative to undifferentiated BJ-iPSC controls at day 15 post differentiation. Gene expression was normalized to *ACTINB* and *GAPDH*. $N = 3$ independent biological differentiations. **(E)** Immunostaining of hiPSC-SNs at various developmental stages exhibiting SN canonical markers, i.e. *PRPH*, *BRN3A* and *ISL1*. **(F)** qPCR analysis in hiPSC-SNs showing upregulation of H1R/TRPV1 signalling pathway elements, i.e. *H1R*, *TRPV1*, *SCN9A* and *SCN11A* relative to undifferentiated BJ-iPSC controls at day 28 post differentiation, respectively. Gene expression was normalized to *ACTINB* and *GAPDH*. $N = 3$ independent biological differentiations. **(G)** Immunostaining of hiPSC-SNs at day 50 demonstrating co-localization of H1R and TRPV1 elements.



indicates that hiPSC-SNs were functionally mature as early as day 30, and were responsive to multiple itch- and pain-related stimuli including histamine, capsaicin and heat (temperature).

TRPV1 mediates histamine-induced stimulation of H1R in a subset of hiPSC-SNs

Previous studies in mice have demonstrated that TRPV1 act downstream of histamine in pruritogenesis^{3,5}, and this may result from the direct binding of H1R to the C-terminus of TRPV1⁸. Since this interaction between H1R and TRPV1 has not been established in human sensory neurons, we used hiPSC-SNs to investigate if the H1R-TRPV1 pruritogenic signaling is conserved in humans. Using calcium imaging, we found that not all hiPSC-SNs respond to both histamine and capsaicin (Fig. 3A). Out of 1044 neurons analyzed, 312 neurons (30%) responded to capsaicin and 238 neurons (23%) responded to histamine, and only 64 neurons (6%) are responsive to both agonists (Fig. 3B).

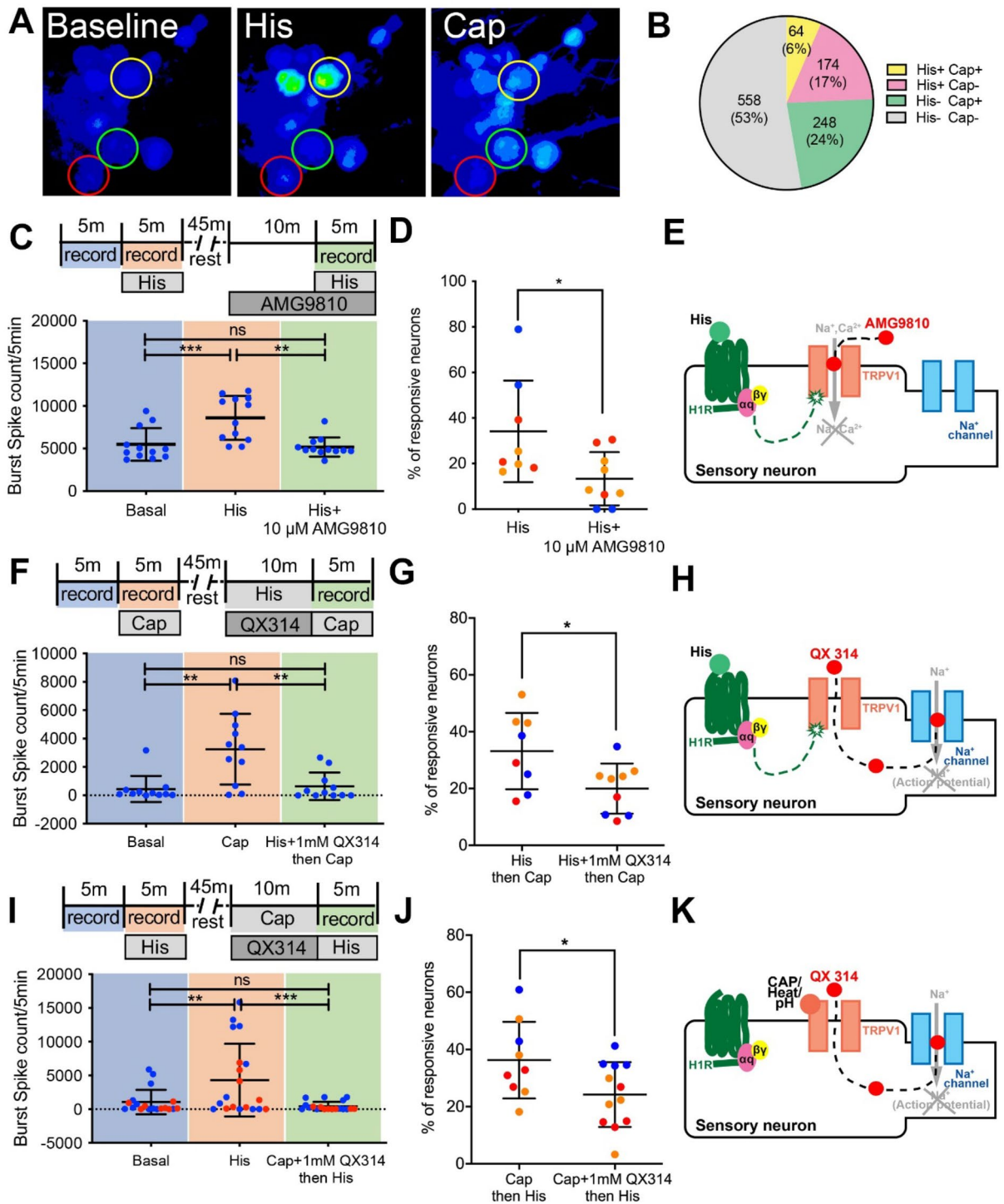
◀ **Fig. 2.** Functional characterization of H1R and TRPV1 in hiPSC-SNs. **(A)** Time trace of fluorescence change in calcium influxes within five representative hiPSC-SNs in response to either H1R agonist, i.e. histamine (His) or TRPV1 agonist, i.e. capsaicin (Cap). **(B, C)** Quantitation of the percentages of neurons responding to histamine or capsaicin in the presence of H1R antagonist, i.e. mepyramine **(B)** or TRPV1 antagonist, i.e. AMG9810 **(C)**, respectively. $N=2-3$ independent biological differentiations (colour coded as blue, red and orange spots). For each independent differentiation, 3–4 technical repeats (spots indicated in same colour) were performed with 60–100 neurons analyzed in each repeat. **(D, E)** Multielectrode array (MEA) measurements demonstrating an increase in hiPSC-SNs' burst spike events in response to stimulation with histamine **(D)** or capsaicin **(E)**. Hyperexcitabilities are reversibly suppressed in the presence of H1R antagonist, i.e. mepyramine **(D)** or TRPV1 antagonist, i.e. AMG9810 when tracked in the same group of neurons. $N=3$ independent biological differentiations (colour coded as blue, red and orange spots). For each independent differentiation, all active electrode channels recording at multiple locations of a single hiPSC culture well are indicated as spots of the same colour. **(F)** Increase in hiPSC-SNs' excitabilities/burst spike count correspond to noxious heat exposure from 37 to 42 °C (1–9 min) and gradually decreases as temperature cools back to 37 °C (9–20 min). Heat response is reversibly ameliorated in the presence of AMG9810. $N=3$ independent biological differentiations but only one representative time course result is shown here. Data is shown as means \pm SD. $^{ns}P > 0.05$, $^*P \leq 0.05$, $^{**}P \leq 0.01$, $^{***}P \leq 0.001$, $^{****}P \leq 0.0001$, unpaired Student T-test **(B, C)** or Friedman test with Dunn's multiple comparisons test **(D, E)**.

Next, we treated hiPSC-SNs with histamine and then measured neuronal network burst activities with and without TRPV1 inhibition. This revealed an increase in burst firing in response to histamine as we established earlier (Fig. 3D), which was attenuated by TRPV1 inhibitor, AMG9810, in both MEA analysis (Fig. 3C) and calcium imaging (Fig. 3D) across single and triplicate biological replicates, respectively, and as illustrated in Fig. 3E. This corroborates with previous findings in mice^{4,5}, and confirms that this H1R-TRPV1 pruritogenic signaling pathway is conserved in humans. We then made use of QX-314, a membrane-impermeable sodium channel blocker, recognized for its ability to selectively inhibit sensory by entering through TRPV1 ion channels^{29–31}. Our findings demonstrated that combining histamine with QX-314 resulted in a reduction of capsaicin response in hiPSC-SNs when assessed by MEA (Fig. 3F) and calcium imaging (Fig. 3G) across single and triplicate biological replicates, respectively. This implies that histamine stimulation triggers the downstream activation of TRPV1 channels and thus influx of QX-314 to silence fibers positive for both H1R and TRPV1 (Fig. 3H). Likewise, combining either capsaicin or a 42 °C heat stimulus with QX-314 resulted in a decreased histamine response in hiPSC-SNs, as assessed by MEA (Fig. 3I and Supplementary Fig. 3) and calcium imaging (Fig. 3J). This supports the notion that histamine operates upstream in TRPV1-mediated signaling and this is perturbed when activated TRPV1 fibers are silenced by QX-314 (Fig. 3K). Altogether, our data shows that hiPSC-SNs are functional and exhibit conserved pruritogenic responses, potentially making these a valuable humanized platform for screening TRPV1 antagonists that have anti-pruritogenic properties.

Multiple TRPV1 antagonists inhibit H1R-mediated neuronal activities

Our data so far supports the use of hiPSC-SN as a discovery and validation platform for the identification of compounds that mediate histamine-dependent itch. To perform further validation, we chose a few TRPV1 antagonists and measured their efficacy in suppressing histamine-induced neuronal burst firing. Here, we examined two sets of TRPV1 antagonists, well-recognized for their hyperthermia-inducing properties, i.e. AMG517 and ABT102 and hyperthermia-free properties, i.e. SB366791, SB705498 and PAC-14,028^{21,32,33}. First, a dose-response assay was performed to determine the ideal in vitro therapeutic dose. Briefly, hiPSC-SNs were exposed to noxious heat to induce neuronal burst firing, and then treated with various concentrations of antagonists to determine for an effective dose which exerted a significant suppressive effect on burst activity (Supplementary Fig. 4). The effective dose was then validated for its ability to suppress capsaicin responses (Fig. 4A–E). Intriguingly, we observed hyperthermic free antagonists SB366791 and SB705498 demonstrating remarkably potent suppressive effects on capsaicin activations across all assessed neuronal populations. Additionally, these inhibitory effects appeared relatively irreversible even in capsaicin stimulations conducted after removal of the antagonists (Fig. 4C, D). In contrast, the suppressive effects of hyperthermic antagonists AMG517 and ABT102 were comparatively inconsistent across neuronal population and reversible following antagonist removal (Fig. 4A, B). When comparing all four antagonists, the inhibitory effect of SB366791 appears most potent at 10 μ M (Fig. 4D and Supplementary Fig. 4).

Thereafter, hiPSC-SNs were treated with 25 μ M histamine, along with TRPV1 antagonists at their therapeutic dose, and neuronal burst activities were measured. Interestingly, we once again observed the hyperthermic free antagonists SB366791 and SB705498 to exhibit higher efficacy in suppressing histamine-induced neuronal activity (Fig. 4H, I) surpassing the impact of hyperthermic antagonists AMG517 and ABT102 (Fig. 4F, G). Notably, SB366791 demonstrated the most robust inhibition at the lowest concentration employed (Fig. 4H). We also tested PAC-14028, a potent TRPV1 antagonist currently in phase III trials for chronic topical treatment of atopic dermatitis (AD)-related pruritus^{19,34}. Consistent with previous report observing attenuation of histamine-mediated itch response by PAC-14028³⁵, PAC-14,028 similarly inhibited both capsaicin (Fig. 4E) and histamine responses (Fig. 4I) effectively in hiPSC-SNs. Taken together, we show that hiPSC-SNs can effectively identify TRPV1 antagonists that can be developed into treatments for histamine-induced itch.



Discussion

Use of TRPV1 antagonists to address histamine-induced itch has gained traction in recent years. Yet, many existing studies that examine the feasibility of this approach rely solely on mammalian models^{7,34,36–38}. Although animal models are crucial, the findings derived from animal studies may not consistently apply to human clinical trials, primarily due to the species-specific nature of TRPV1 channels²¹. This present study is therefore the first to utilize a physiologically relevant human in vitro model to investigate the interrelation between H1R and TRPV1 signalling and prove that they are conserved in human sensory neurons as with their mammalian counterparts.

Here, we show with immunohistochemistry staining that H1R is co-expressed with TRPV1 in sensory neurons derived from hiPSCs. The expressed channels are functional, exhibiting both spontaneous and stimulated electrical responses to their corresponding agonists and antagonists as early as day 28 and lasting till day 70. Calcium imaging revealed a subset of cells showing responses to both stimuli. Consistent with this, use of an MEA-based assessment which measures neuronal activities on a network level similarly observed a decrease in histamine response after TRPV1 neurons were either blocked by TRPV1 antagonist or silenced by targeted

◀ **Fig. 3.** H1R signals through TRPV1 in a proportion of hiPSC-SNs. **(A,B)** Fluorescence images of calcium response at baseline and after applications of histamine and capsaicin **(A)** and pie chart showing the proportion of SNs that responded to either or both agonists **(B)**. $N=6$ independent biological differentiations. For each independent differentiation, 2–4 technical repeats were performed with 40–140 neurons analyzed in each repeat. **(C–E)** Histamine-mediated activation of H1R is inhibited in the presence of a TRPV1 antagonist, i.e. AMG9810 as shown in a MEA measurement **(C)**, calcium imaging **(D)** and schematic illustration **(E)**. **(F–H)** Co-administration of histamine and sodium channel blocker, i.e. QX-314 followed by a subsequent stimulation with capsaicin reveals a suppression in capsaicin response in both MEA analysis **(F)**, calcium imaging **(G)** and schematic illustration **(H)**. **(I–K)** Co-administration of capsaicin and sodium channel blocker, i.e. QX-314 followed by a subsequent stimulation with histamine reveals a suppression in histamine response in both MEA analysis **(I)**, calcium imaging **(J)** and schematic illustration **(K)**. Data is shown as means \pm SD. $^{ns}P > 0.05$, $^{*}P \leq 0.05$, $^{**}P \leq 0.01$, $^{***}P \leq 0.001$, $^{****}P \leq 0.0001$, Friedman test with Dunn's multiple comparisons test **(C,F,I)**, Mann-Whitney test **(D)** or unpaired Student T-test **(G, J)**. $N=1-3$ independent biological differentiations (colour coded as blue, red and orange spots) in all experimental set-ups described in **(C–K)**. For each independent differentiation described in MEA experiments **(C,F,I)**, active electrode channels recording at multiple locations of a single hiPSC culture well are indicated as spots of the same colour. For each independent differentiation described in calcium experiments **(D,G,J)**, 3–4 technical repeats (spots indicated in same colour) were performed with 35–150 neurons analyzed in each repeat.

delivery of a sodium channel blocker. Likewise, silencing of H1R neurons diminished capsaicin response. This reinforces the notion that hiPSC-SNs exhibit conserved H1R-TRPV1 signaling pathways, making them a potential platform for screening TRPV1 antagonists with anti-pruritogenic properties against histaminergic itch.

As a proof-of-concept, our work is the first to use an in vitro human sensory neurons as a platform combined with the means to perform multi-site measurements with the MEA, to screen TRPV1 antagonists by their effectiveness to block histamine activation. To this end, we tested two known hyperthermic (i.e. AMG517 and ABT102) and three known thermal neutral (i.e. SB366791, SB705498 and PAC-14028) TRPV1 antagonists and determined their effective doses to block two modes of TRPV1 activation by heating and capsaicin. Remarkably, our findings supported an earlier observation indicating that, although thermal neutral SB366791 exhibited inefficiency in inhibiting the heat activation of rat TRPV1 compared to hyperthermic AMG9810, their inhibitory potencies were comparable in Chinese hamster ovary cells with stable expression of human TRPV1³⁹. This underscores the importance of employing a humanized model, like ours, to differentiate the species-specific heat activation threshold of TRPV1. Garami et al.²¹ had earlier proposed the hypothesis that the hyperthermic response to TRPV1 antagonists in humans is closely tied to heightened sensitivity to changes in potency in the proton and heat modes, with the capsaicin mode being less relevant. Our observation of similar potencies for SB366791 and AMG9810 in blocking heat and capsaicin activation modes potentially implies that the hyperthermic effect of AMG9810 may primarily result from varying inhibitory potencies against the proton activation mode of TRPV1 instead. While this has not been explored in this study, it could serve as a potential focus for future research.

Our in vitro human sensory neuron model also offers the advantage of assessing the inhibition potencies of different TRPV1 antagonists against histamine activation under simulated endogenous conditions. This noteworthy feature holds valuable potential for predicting the actual performance of these antagonists in human clinical trials. In support of this, our study found a lower potency with SB705498 to block histamine activation and this was corroborated by a human clinical trial study showing that topical application of SB705498 yielded insignificant symptomatic benefit for histaminergic induced itch⁴⁰. We also examined Asivatrep (PAC-14028), a TRPV1 antagonist presently undergoing phase III trials for chronic management of atopic dermatitis (AD)-associated itching^{19,34}. We successfully reproduced its capability to inhibit both capsaicin and histamine stimulations, providing additional support for the efficacy of our model.

A promising candidate identified through our proof-of-concept screen is SB366791, surpassing all TRPV1 antagonists in blocking both heat and capsaicin modes of TRPV1, as well as histamine activations, with the highest potency. We hypothesize that SB366791's exceptional potency may be attributed to its inhibitory effect possibly extending beyond H1R to encompass H4R. This is supported by observations from the study by Wilzopolski et al., which presented in vitro evidence showcasing SB366791's dose-dependent reduction of intracellular calcium increases in mouse DRGs stimulated with either a pan-H1-4R agonist (histamine) or an H4R agonist (ST-1006). Additionally, their in vivo findings demonstrated that SB366791 attenuated itch induced by the H4R agonist (ST-1006), a response not achieved by another TRPV1 antagonist, Capsazepine⁷. Notably, since SB366791 is thermal neutral, its mode of administration could conceivably expand beyond topical application which limits its effectiveness to a local area. Accordingly, the feasibility of an intrathecal administration has been recently explored in a mouse model where SB366791 was shown to reduce morphine-induced itch without causing hyperthermia⁴¹.

Conclusions

In conclusion, this study presents evidence that TRPV1 acts downstream of H1R in a human model of iPSC-derived sensory neurons as with in mammalian models. In a proof-of-concept investigation, the utilization of our hiPSC-SNs platform in conjunction with MEA read-outs offers a novel and sensitive approach to large-scale screening of TRPV1 antagonists. This physiologically relevant model is particularly valuable considering the challenges associated with species-specificity when employing mammalian TRPV1. Notably, we demonstrate

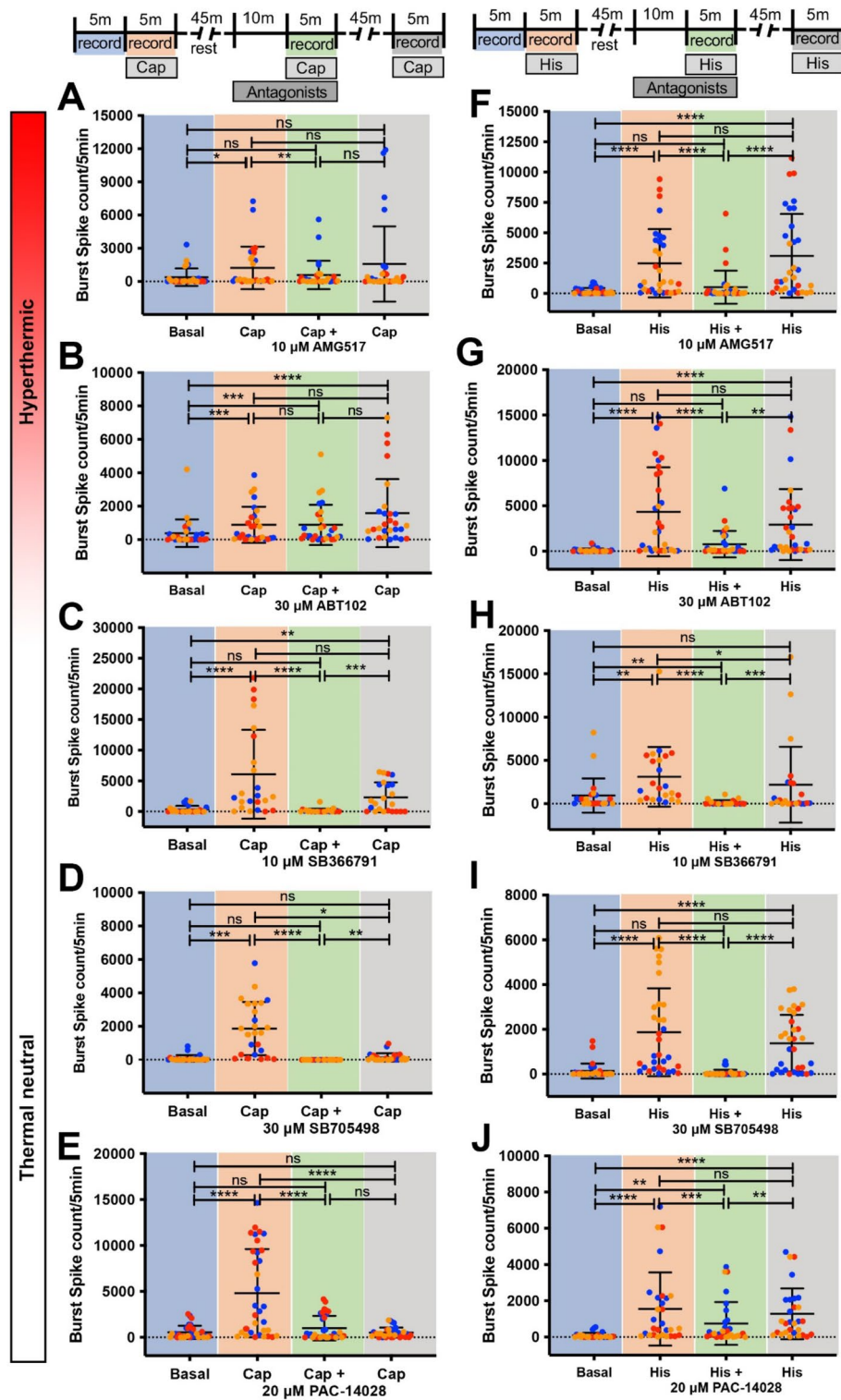


Fig. 4. Efficacies of various TRPV1 antagonists to block capsaicin and histamine activations in hiPSC-SNs. (A–E) MEA based assessments of hyperthermia-inducing TRPV1 antagonists, i.e. AMG517 (A) and ABT102 (B) and hyperthermia-free TRPV1 antagonists, i.e. SB366791 (C), SB705498 (D) and PAC-14,028 (E) on TRPV1 blockage in capsaicin activation mode. (F–J) Effect of hyperthermia-inducing TRPV1 antagonists, i.e. AMG517 (F) and ABT102 (G) and hyperthermia-free TRPV1 antagonists, i.e. SB366791 (H), SB705498 (I) and PAC-14,028 (J) in blocking acute effects of histamine-mediated H1R activation. Data is shown as means \pm SD. $^{ns}P > 0.05$, $^{*}P \leq 0.05$, $^{**}P \leq 0.01$, $^{***}P \leq 0.001$, $^{****}P \leq 0.0001$, Friedman test with Dunn’s multiple comparisons test, $N = 3$ independent biological differentiations in all experimental set-ups (colour coded as blue, red and orange spots). For each independent differentiation, all active electrode channels recording at multiple locations of a single hiPSC culture well are indicated as spots of the same colour.

that, while the tested TRPV1 antagonists are generally effective in blocking histamine activation, they display varying inhibitory potencies. This variability may have predictive implications for their performance in future clinical studies. Subsequent investigations could explore whether our system can also anticipate the hyperthermic effects of TRPV1 antagonists based on their potencies in the proton activation mode.

Data availability

Data availability: The authors declare that all data supporting the findings of this study are available within the article and its supplementary information files or from the corresponding author upon reasonable request. Single-cell RNA-seq data is available via Gene Expression Omnibus accession code GSE256435.

Received: 15 February 2024; Accepted: 5 December 2024

Published online: 28 December 2024

References

- Xie, Z. & Hu, H. TRP channels as drug targets to relieve itch. *Pharmaceuticals (Basel)* **11**, 4 (2018).
- Kahremany, S. et al. Advances in understanding the initial steps of pruritoceptive itch: how the itch hits the switch. *Int. J. Mol. Sci.* **21**, 14 (2020).
- Imamachi, N. et al. TRPV1-expressing primary afferents generate behavioral responses to pruritogens via multiple mechanisms. *Proc. Natl. Acad. Sci. U.S.A.* **106**(27), 11330–11335 (2009).
- Kim, B. M. et al. Histamine-induced Ca^{2+} influx via the PLA(2)/lipoxygenase/TRPV1 pathway in rat sensory neurons. *Neurosci. Lett.* **361**(1–3), 159–162 (2004).
- Shim, W. S. et al. TRPV1 mediates histamine-induced itching via the activation of phospholipase A2 and 12-lipoxygenase. *J. Neurosci.* **27**(9), 2331–2337 (2007).
- Kim, S. et al. Facilitation of TRPV4 by TRPV1 is required for itch transmission in some sensory neuron populations. *Sci. Signal.* **9**(437), 71 (2016).
- Wilzopolski, J. et al. TRPV1 and TRPA1 channels are both involved downstream of histamine-induced itch. *Biomolecules* **11**(8) (2021).
- Gao, Y. et al. TRPV1 SUMOylation suppresses itch by inhibiting TRPV1 interaction with H1 receptors. *Cell. Rep.* **39**(11), 110972 (2022).
- Haberberger, R. V. et al. Human dorsal root ganglia. *Front. Cell. Neurosci.* **13**, 271 (2019).
- Nguyen, M. Q. et al. Single-nucleus transcriptomic analysis of human dorsal root ganglion neurons. *Elife* **10**, 1 (2021).
- Tavares-Ferreira, D. et al. Spatial transcriptomics of dorsal root ganglia identifies molecular signatures of human nociceptors. *Sci. Transl. Med.* **14**(632), eabj8186 (2022).
- Jung, M. et al. Cross-species transcriptomic atlas of dorsal root ganglia reveals species-specific programs for sensory function. *Nat. Commun.* **14**(1), 366 (2023).
- Alshawaf, A. J. et al. Phenotypic and functional characterization of peripheral sensory neurons derived from human embryonic stem cells. *Sci. Rep.* **8**(1), 603 (2018).
- Chambers, S. M. et al. Combined small-molecule inhibition accelerates developmental timing and converts human pluripotent stem cells into nociceptors. *Nat. Biotechnol.* **30**(7), 715–720 (2012).
- Eberhardt, E. et al. Pattern of functional TTX-resistant sodium channels reveals a developmental stage of human iPSC- and ESC-derived nociceptors. *Stem Cell. Rep.* **5**(3), 305–313 (2015).
- Guimaraes, M. Z. P. et al. Generation of iPSC-derived human peripheral sensory neurons releasing substance P elicited by TRPV1 agonists. *Front. Mol. Neurosci.* **11**, 277 (2018).
- Cevikbas, F. et al. A sensory neuron-expressed IL-31 receptor mediates T helper cell-dependent itch: involvement of TRPV1 and TRPA1. *J. Allergy Clin. Immunol.* **133**(2), 448–460 (2014).
- Andersen, H. H. et al. Antipruritic effect of pretreatment with topical capsaicin 8% on histamine- and cowhage-evoked itch in healthy volunteers: a randomized, vehicle-controlled, proof-of-concept trial. *Br. J. Dermatol.* **177**(1), 107–116 (2017).
- Park, C. W. et al. Asivatrep, a TRPV1 antagonist, for the topical treatment of atopic dermatitis: phase 3, randomized, vehicle-controlled study (CAPTAIN-AD). *J. Allergy Clin. Immunol.* **149**(4), 1340–1347 (2022).
- Roblin, D. et al. Topical TrkA kinase inhibitor CT327 is an effective, novel therapy for the treatment of pruritus due to psoriasis: results from experimental studies, and efficacy and safety of CT327 in a phase 2b clinical trial in patients with psoriasis. *Acta Derm. Venereol.* **95**(5), 542–548 (2015).
- Garami, A. et al. Hyperthermia induced by transient receptor potential vanilloid-1 (TRPV1) antagonists in human clinical trials: insights from mathematical modeling and meta-analysis. *Pharmacol. Ther.* **208**, 107474 (2020).
- Garami, A. et al. Contributions of different modes of TRPV1 activation to TRPV1 antagonist-induced hyperthermia. *J. Neurosci.* **30**(4), 1435–1440 (2010).
- Warren, L. et al. Highly efficient reprogramming to pluripotency and directed differentiation of human cells with synthetic modified mRNA. *Cell. Stem Cell.* **7**(5), 618–630 (2010).
- Tay, S. H. et al. Generation of cortical, dopaminergic, motor, and sensory neurons from human pluripotent stem cells. *Methods Mol. Biol.* **2549**, 359–377 (2022).
- Satija, R. et al. Spatial reconstruction of single-cell gene expression data. *Nat. Biotechnol.* **33**(5), 495–502 (2015).
- Bataille, A. et al. In vitro differentiation of human skin-derived cells into functional sensory neurons-like. *Cells* **9**, 4 (2020).
- Blanchard, J. W. et al. Selective conversion of fibroblasts into peripheral sensory neurons. *Nat. Neurosci.* **18**(1), 25–35 (2015).
- Xiong, C. et al. Human induced pluripotent stem cell derived sensory neurons are sensitive to the neurotoxic effects of paclitaxel. *Clin. Transl. Sci.* **14**(2), 568–581 (2021).
- Binshtok, A. M., Bean, B. P. & Woolf, C. J. Inhibition of nociceptors by TRPV1-mediated entry of impermeant sodium channel blockers. *Nature* **449**(7162), 607–610 (2007).
- Roberson, D. P. et al. Activity-dependent silencing reveals functionally distinct itch-generating sensory neurons. *Nat. Neurosci.* **16**(7), 910–918 (2013).
- Stueber, T. et al. Quaternary lidocaine derivative QX-314 activates and permeates human TRPV1 and TRPA1 to produce inhibition of sodium channels and cytotoxicity. *Anesthesiology* **124**(5), 1153–1165 (2016).
- Gavva, N. R. et al. The vanilloid receptor TRPV1 is tonically activated in vivo and involved in body temperature regulation. *J. Neurosci.* **27**(13), 3366–3374 (2007).
- Gavva, N. R. et al. Pharmacological blockade of the vanilloid receptor TRPV1 elicits marked hyperthermia in humans. *Pain* **136**(1–2), 202–210 (2008).
- Lee, J. H. et al. A novel, topical, nonsteroidal, TRPV1 antagonist, PAC-14028 cream improves skin barrier function and exerts anti-inflammatory action through modulating epidermal differentiation markers and suppressing Th2 cytokines in atopic dermatitis. *J. Dermatol. Sci.* **1**, 1 (2018).

35. Yun, J. W. et al. Antipruritic effects of TRPV1 antagonist in murine atopic dermatitis and itching models. *J. Investig. Dermatol.* **131**(7), 1576–1579 (2011).
36. Jian, T. et al. TRPV1 and PLC participate in histamine H4 receptor-induced itch. *Neural Plast.* **2016**, 1682972 (2016).
37. Tsagareli, M. G. et al. Thermal hyperalgesia and mechanical allodynia elicited by histamine and non-histaminergic itch mediators: respective involvement of TRPV1 and TRPA1. *Neuroscience* **449**, 35–45 (2020).
38. Yang, N. et al. Desensitization of TRPV1 involved in the antipruritic effect of osthole on histamine-induced scratching behavior in mice. *Evid. Based Complement Altern. Med.* 4012812 (2021).
39. Gavva, N. R. et al. AMG 9810 [(E)-3-(4-t-butylphenyl)-N-(2,3-dihydrobenzo[b][1,4] dioxin-6-yl)acrylamide], a novel vanilloid receptor 1 (TRPV1) antagonist with antihyperalgesic properties. *J. Pharmacol. Exp. Ther.* **313**(1), 474–484 (2005).
40. Gibson, R. A. et al. A randomised trial evaluating the effects of the TRPV1 antagonist SB705498 on pruritus induced by histamine, and cowhage challenge in healthy volunteers. *PLoS ONE* **9**(7), e100610 (2014).
41. Sakakibara, S. et al. Effects of an intrathecal TRPV1 antagonist, SB366791, on morphine-induced itch, body temperature, and antinociception in mice. *J. Pain Res.* **12**, 2629–2636 (2019).

Acknowledgements

The authors would like to thank Singapore Bioimaging Consortium (SBIC)-Nikon Imaging Centre at Biopolis, Central Imaging Facility (CIF) and Singleron Biotechnologies for the use of their equipment and technical support in this study.

Author contributions

SHT and SYN conceptualized the study and wrote the manuscript. SHT, WN, CYN and ZSC performed the experiments while SHT, JKSP, CYN, ZJK and BSS performed the analyses. All authors reviewed and edited the manuscript.

Funding

This research was funded by the A*STAR RIE2020 Advanced Manufacturing and Engineering Programmatic Grant (AMBM), the A*STAR Confirma Programme and the Institute of Molecular and Cell Biology, A*STAR.

Declarations

Competing interests

The authors declare no competing interests.

Additional information

Supplementary Information The online version contains supplementary material available at <https://doi.org/10.1038/s41598-024-82549-7>.

Correspondence and requests for materials should be addressed to S.-Y.N.

Reprints and permissions information is available at www.nature.com/reprints.

Publisher's note Springer Nature remains neutral with regard to jurisdictional claims in published maps and institutional affiliations.

Open Access This article is licensed under a Creative Commons Attribution-NonCommercial-NoDerivatives 4.0 International License, which permits any non-commercial use, sharing, distribution and reproduction in any medium or format, as long as you give appropriate credit to the original author(s) and the source, provide a link to the Creative Commons licence, and indicate if you modified the licensed material. You do not have permission under this licence to share adapted material derived from this article or parts of it. The images or other third party material in this article are included in the article's Creative Commons licence, unless indicated otherwise in a credit line to the material. If material is not included in the article's Creative Commons licence and your intended use is not permitted by statutory regulation or exceeds the permitted use, you will need to obtain permission directly from the copyright holder. To view a copy of this licence, visit <http://creativecommons.org/licenses/by-nc-nd/4.0/>.

© The Author(s) 2024